Surface Plasmons of Finite Nanoring Arrays

M. El-Shenawee[1], P. Blake[2], A. M. Hassan[1] and D.K. Roper[2]
[1]Department of Electrical Engineering
[2]Department of Chemical Engineering
University of Arkansas
Fayetteville, AR, USA
magda@uark.edu, pblake@uark.edu

***Abstract*—Numerical and fabrication investigations of gold nanoring finite arrays are presented. Surface plasmon resonances are computed using the method of moment surface integral equation. The nanoring arrays are fabrication via electron beam lithography templating and electroless gold plating. The results show the change of surface plasmons resonances, to larger wavelengths, when the nanoring thickness decreases. Also, the array size and the separation distance factors influence the amplitude of the extinction coefficients along with the resonance wavelength.**

Keywords-nanotoroid, surface plasmons, method of moments, electron beam lithography,nanorings.

I. INTRODUCTION

Nanorings exhibit unique plasmon properties that could improve low photocurrent generation in photovoltaics (PV), which currently prevents cost-effective mass production and use of PV for sustainable solar energy. Plasmons are oscillating free electrons confined to metal surfaces excited by incident hυ at specific wavelengths. The objective of this work has been to model, fabricate and characterize gold (Au) nanoring (NR) structures.

II. METHODOLOGY

A. The Numerical Method

The three dimensional method of moments implementation of the surface integral equation (MoM/SI) is employed to calculate the plasmon resonances of a finite array immersed in air [1]. A parallelized version of the conventional method of moment computer code is excecuted on the Star of Arkansas Supercomputer. The nanoring array sizes ranged from 2×2 to 6×6 elements. The extinction and scattering coefficinets were claculated as funtions of wavelength. The gold experimental properties of Johnson *et al* are adopted here [2]. Plane waves travelling in the *z*-direction with *y*-polarized fields are assumed in this work.

The extinction coefficient's asymptotic expression is given by [3]:

$$C_{ext} = 2\lambda \mathrm{Img}\left(\tilde{\tilde{E}}^{inc} \cdot \tilde{\tilde{E}}^{sca} \Big|_{\hat{n}^{sca}=\hat{n}^{inc}} \right) \qquad (1)$$

where $\overline{E}^{inc} = \tilde{\tilde{E}}^{inc}(e^{jk_0 r}/r)$ and $\overline{E}^{sca} = \tilde{\tilde{E}}^{sca}(e^{jk_0 r}/r)$, are the incident and scattered electric fields, respectively, $\hat{n}^{inc}$ and $\hat{n}^{sca}$ are the unit vectors in the incident and scatter directions, respectively, λ is the wavelength in the surrounding medium, k_0 is the wavenumber, and r is the distance from the origin.

Calculating the extinction, absorbing and/or scattering coefficients versus the wavelength can be categorized as an *embarrassingly parallel* problem since the calculation of the coefficients at each wavelength is entirely independent of the other wavelengths. Therefore, the Message Passing Interface (MPI) can be easily utilized such that the calculation of the coefficients is performed in parallel rather than in serial; one wavelength after the other. Ideally, each processor should calculate the coefficients at only one wavelength and in this case, a speed up of almost *N* will be achieved where *N* is the number of wavelengths in the spectrum of interest. However, due to the limited number of processors, each processor is typically programmed to simulate *M* wavelengths with a resulting speedup of *N*/*M*. Other requirements such as the amount of available memory also need to be considered. For example, the supercomputer at the University of Arkansas, Star of Arkansas, has a node with four twelve-core AMD 2.2 GHz processors, 4x12 MB cache, and a total of 256GB of memory. The calculation of the coefficients at one wavelength for of a 6×6 array requires 30 GB of memory and, therefore, only 8 wavelengths, and 8 processors out of the available 48, can be running in parallel on this node. This results in a speed up of 8 times which still provides a significant saving in computational time with minimal parallelization effort.

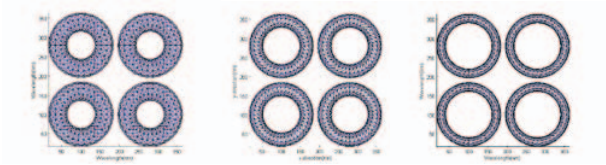

Fig. 1 Three 2×2 nanoring arrays of outer diameter 164 nm and inner diameter of (a) 72 nm, (b) 96 nm, and (c) 120 nm, respectively.

This work is sponsored by NSF award # 1006927

B. The Fabrication and CharacterizationTechnique

(1) Electron Beam Lithography Pattern Generation: Regular arrays of gold nanorings (AuNRs) were fabricated using electron beam lithography (EBL) and electroless gold plating [4]-[7]. EBL was performed using a Philips XL 30 environmental scanning electron microscope (SEM) (FEI, Hillsboro, OR) equipped with a Nanometer Pattern Generation System to control array properties such as nanoparticle size and spacing. A 100.5µm×100.5µm square array of filled circles with a center-to-center horizontal and vertical spacing of 670 nm (total size 502.5µm×502.5µm) is fabricated.

(2) Gold Nanoring Characterization (AuNRs): The ability to fabricate AuNRs of various size and aspect ratios was analyzed using the same SEM microscope used for EBL. AuNRs with an outer diameter of 99.6 ± 5.2, 130.8 ± 26.4, 207.0 ± 11.5, and 262.3 ± 6.8 nm were obtained. Images of representative AuNRs for each of these samples will be shown in Section III. Some inherent difficulties with this fabrication method are related to the method used to plate the Au to the surface of the EBL patterned substrate, especially when the NR outer diameter is smaller than 100 nm. Another defect occurs when some of the removed Au is re-deposited on the substrate surface.

III. Numerical Results

A. Computer Simulations

The extinction coefficient C_{ext} in (1) is plotted versus the wavelenth from 400 nm to 1300 nm for varius nanoring arrays as shown in Figs. 2a-d. In all cases, the separation distance, measured between the centers of nanorings, is assumed d = 95nm, unless otherwise mentioned. All nanorings are made of gold in this work.

Fig. 2a shows C_{ext} for three 2×2 nanoring arrays of outer diameter D_o = 164 nm and inner diameters D_i = 72 nm, 96 nm, and 120 nm, respectively. The results show that the surface Plasmon resonance wavelength increases as the thickness of the nanoring decreases. The same observation is demonstrated in Fig. 2b but for 4×4 arrays of smaller size where D_o = 84 nm and D_i = 22 nm, 42 nm, and 60 nm, respectively. The results of Fig. 2c show sharper peaks compared with those in Fig. 2a which is, as anticipated, due to the increase of the number of elements in the array from 4 elements in Fig. 2a to 16 elements in Fig. 2b. However, the results of Fig. 2a show the resonance of a higher order mode in the three considered nanoring sizes.

Fig. 2c shows C_{ext} of several array sizes of 1 × 2, 2 × 2, 4 × 4, 5 × 5, and 6 × 6. All nanorings have inner and outer diameters of 42 nm and 84 nm, respectively, with separation distance of 95 nm. The extinction coefficient of a single nanoring is shown as a reference. The results clearly show the increase in the amplitude and shift in surface Plasmon resonances as the number of elements in the array increases from one to thirty six elements.

Fig. 2d shows results for the 6 × 6 array with two different separation distance d = 0 (touching nanorings), d = 95 nm, and d = 640 nm. The result of a single nanoring is included as a reference. The results show that as the separation distance decreases, the wavelength of the surface Plasmon increases. For example, the resonance wavelength is ~ 680 nm for d = 640 nm, ~750 nm for d = 95 nm, and ~880 nm for d = 0. It is observed in Fig. 2d, as anticipated, that when the nanorings are far from each other, the extinction coefficient of the array is almost the exact accumulation of that due to a single nanoring. The curve in red color represents the extinction coefficient of the 36 array elements, while the comparable green curve represents the extinction coefficient of the single nanoring multiplied by 36. The two curves are in excellent agreement with each other, which is not the case of the curves when d =0 or d = 95nm. The results of d = 320 nm show similar observation of the d = 640 nm case (not presented). The fabrication results show challenging issues when the nanorings are close to each other, i.e. when the separation distance is a sub-wavelength.

The results of Fig. 2f show the extinction coefficients of two 4×4 nanoring arrays; one is uniform where all nanorings have the same inner and outer diameters of 42 nm and 84 nm, respectively, with separation distance of 95 nm. The second array also consists of 16 elements but of random inner and outer diameters and hence random separation distance. The nonuniform array is shown in Fig. 2g. The results of Fig. 2f show multiple surface plasmons correspond to the multiple sizes of nanorings in the array. Due to the small separation distance between the nanorings, there are interactions that lead to un-separated resonances.

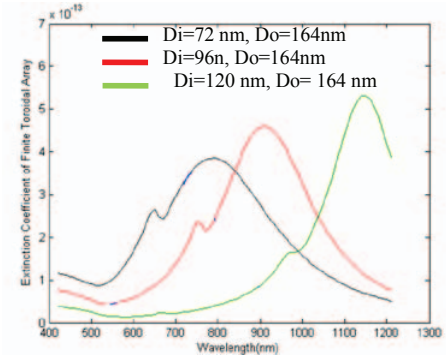

Fig. 2a The extinction coefficient vs wavelength for 2×2 nanoring arrays of Fig. 1 with separation gap d = 95 nm.

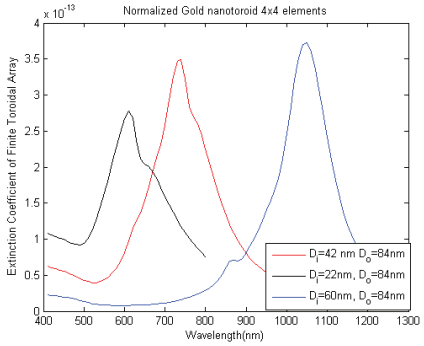

Fig. 2b The extinction coefficient vs wavelength for 4×4 nanoring arrays of outer diameter 84 nm and inner diameters of 22 nm, 42 nm, and 60 nm. The separation gap d = 95 nm.

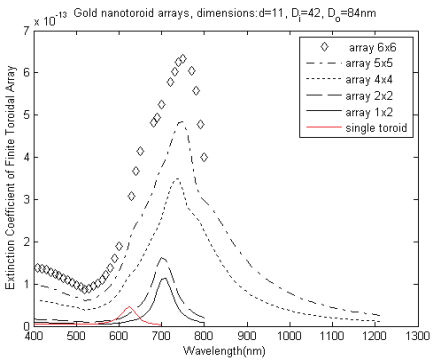

Fig. 2c The extinction coefficient vs wavelength for nanoring arrays of outer diameter 84 nm and inner diameters of 42 nm and d = 95 nm.

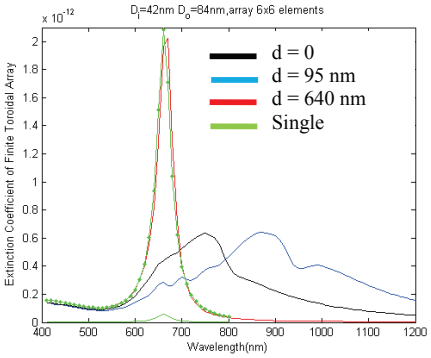

Fig. 2d The extinction coefficient vs wavelength for 6×6 nanoring arrays of outer diameter 84 nm and inner diameters of 42 nm with d = 0, 95 nm, and 640 nm.

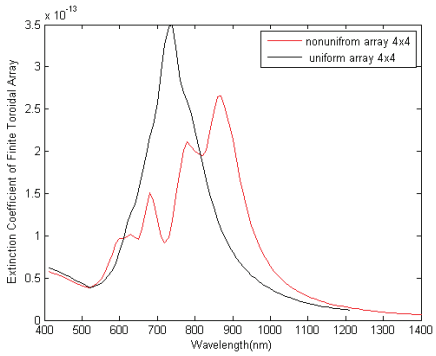

Fig. 2f The extinction coefficient vs wavelength for 4×4 nanoring arrays with random separation gap and inner and outer radii of nanorings (nonuniform) vs 4×4 nanoring array with inner and outer diameters of 42 nm and 84 nm, respectively, and d =95nm (uniform).

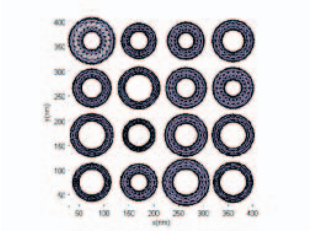

Fig. 2g Nonuniform of 16 nanorings of random inner and outer diameters.

B. Fabrication Methods

(1) Assembly Methods: NP spheres have been previously assembled in random configurations on Si by deposition using pulsed lasers, electrochemistry, and microwaves; by self-assembly on thiols, dendrimers or other polymers; by conjugation to polymers; by evaporation; and by heating evaporated film via resistivity or convection. But time needed to deposit or self-assemble NP sizes 25≤ r ≤100 nm is long due to low available NP concentrations and diffusion. No prior solution methods are available to make nano-antennae like rings, which precludes deposition or self-assembly. Conjugation, evaporation, and heating produce irregular NP assemblies, and oblate hemispheroids, not nano-antennae.

(2) Top-down Methods: Regular arrays of Au chains, elliptical, or bean-shaped NPs and nanodisks have been created by AFM tip manipulation, nanosphere lithography (NSL) combined with reactive ion etching (RIE), and EBL. EBL, in particular, offers the ability to create nanostructures with dimensions given by the width of the beam in patterned features on the electron resist. EBL is commonly used to template cylindrical holes in PMMA in which to evaporate or sputter metal thin films to produce metal cylinders. But structures formed by these methods have sharp edges, not spheroidal ones. EBL is used to template cylindrical holes in PMMA to evaporate or sputter metal thin films to produce metal cylinders. But evaporated or sputtered Au bonds weakly to Si, precluding thermal annealing to spheres.

*(3)Wet-chemistry methods:*Our group recently produced stable, random monomodal assemblies of spherical NPs from 9.5 to 266 nm at densities up to 2.6 x 10^{11} cm^{-2} from Au films made via electroless (EL) plating (see Fig. 3). Unlike evaporation or electroplating, EL plating rapidly forms thermal- and ion-stable Au film at ambient conditions without conductive substrates or costly equipment.

(4) EBL + wet-chemistry for NR lattices: In this work, we fabricated stable, square arrays of Au NP hollow cylinders as illustrated in Fig 3. Square lattices were templated onto PMMA over indium-tin oxide (ITO)-coated Si using EBL. Typical gold deposition using gold evaporation for these patterned features would result in solid nanopillars. AuNRs

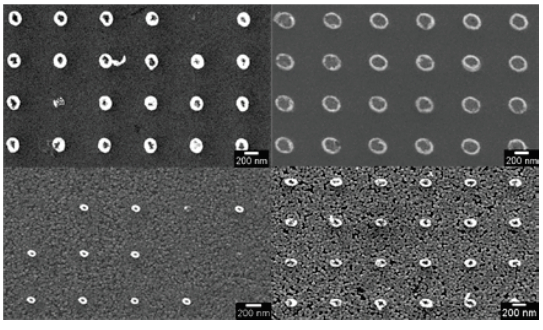

Fig. 3 AuNRs with varied diameter and aspect ratio fabricated using electroless gold plating.

formed using EL gold plating been proven to produce nanorings [6] Heating these nanocylinders 3 x 1 min at 800 ºC annealed them into NR. A 2nd thermal treatment ultimately resulted in a square lattice of NP spheres.

Fabrication of nanoring ring arrays like those in Fig 3 that are more closely-spaced to match the simulations like those in Figures 1 and 2g is currently in progress. These arrays will permit spectroscopic characterization to compare with spectra in Figs 2a-f. Correlation of theoretical models with spectral characterization of fabricated nanorings will be influenced by reproducibility of physical features of elements in the fabricated arrays Defects such as missing, deformed, or partial NRs will negatively influence cross-correlation. The number of such defects can increase as the size of the NRs decreases,

Fabrication is also constrained by the ability of existing methods to produce the NR features of specified size and aspect ratio. For example, NR with outer diameters smaller than 100 nm are challenging to fabricate using even the most sophistacted top-down equipment. Nanoring aspect ratios that are attainable by current fabrication techniques are currently limited on the high end by the uniformity and grain size of gold particles formed.

As an example, AuNR fabricated by electroless plating onto polymethylmethacrylate templates exhibit a granular structure, as illustrated in Fig 4. Average size of these grains was found to be 26.2 ± 3.2 nm, which is directly related to the NR wall thickness.

Electroless plating provides an advantage relative to conventional techniques in this area, in spite of the coagulatory nature of the image in Figure 4. Recent improvements in the control of EL plating have been shown to provide smaller grain sizes, and more uniform deposition of gold films than sputtering or evaporation [8]. A new method to balance redox potential of the wet chemical solutions employed in the electroless gold plating process should assist in controlling deposition and therefore uniformity and grain size. [9].

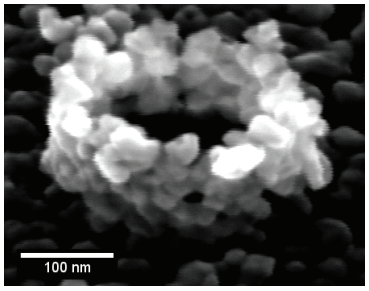

Fig. 4: SEM image of gold nanoring at viewed at 45°.

IV. CONCLUSIONS

The preliminary simulation results obtained in this work, for finite arrays of nanorings, show the dependence of the surface plasmons on the array size, the inner and out diameters of nanoring, and also on the separation distance between these nanorings. Although all results in this work are for nanoring arrays immersed in air, they still provide understanding of several observed issues in the fabricated structures. In addition, these numerical results can guide the fabrication process and foresee issues before starting the process.

ACKNOWLEDGMENT

The authors would like to thank the technical staff of Star Arkansas and the Electron Optics Facility for their help and support of this work. This work is supported in part by the NSF Cybe infrastructure awards EP-0918970 (CI TRAIN) and MRI-072265 (Star of Arkansas) and in part by the Doctoral Academy Fellowship at the University of Arkansas.

REFERENCES

[1] M. El-Shenawee, "Polarization Dependence of Plasmonic Nanotoroid Dimer Antenna," *IEEE Antennas and Wireless Propagation Letters*, vol. 9, pp. 463-466, 2010.

[2] P. B. Johnson and R. W. Christy, "Optical constants of the Noble Metals," *Phys. Rev. B*, vol. 6, no. 12, 1972.

[3] C. F. Bohren and D. R. Huffman, Absorption, and Scattering of Light by Small Particles, *John Wiley & Sons*, 1983.

[4] W. Ahn, P. Blake, J. Shultz, M.E. Ware, and D.K. Roper, "Fabrication of regular arrays of gold nanospheres by thermal transformation of electroless-plated films," *J. Vac. Sci. Technol. B*, vol. 28, pp. 638-642, May/Jun. 2010.

[5] W. Hu, K. Sarveswaran, M. Lieberman, and G.H. Bernstein, "Sub-10 nm electron beam lithography using cold development of poly(methylmethacrylate)," *J. Vac. Sci. Technol. B*, vol. 22, pp. 1711-1716, Jul/Aug 2004.

[6] P. Blake, W. Ahn, and D.K. Roper, "Enhanced uniformity in arrays of electroless plated spherical gold nanoparticles using tin presensitization," *Langmuir*, vol. 26, pp. 1533-1538, 2010.

[7] W. Ahn, B. Taylor, A.G. Dall'Asén, and D.K. Roper, "Electroless gold island films: photoluminescence and thermal transformation to nanoparticle ensembles," *Langmuir*, vol. 24, pp. 4174–4184, 2008.

[8] Jang, G.-G. and D.K. Roper, "Continuous flow electroless plating enhances optical features of Au films and nanoparticles," *J. Phys. Chem C. pp.* 113:19228-19236, 2009

[9] Jang, G.-G. and D.K. Roper., "Balancing redox activity allows spectrophotometric detection of Au(I) using tetramethylbenzidine dihydrochloride," *Anal. Chem.* (2011) Accepted.